Mechanical and acoustic properties of weakly cemented granular rocks

S. Nakagawa & L. R. Myer
Earth Sciences Division, E.O.Lawrence Berkeley National Laboratory, Berkeley, CA, US

ABSTRACT: This paper presents the results of laboratory measurements on the mechanical and acoustic properties of weakly cemented granular rock. Artificial rock samples were fabricated by cementing sand and glass beads with sodium silicate binder. During uniaxial compression tests, the rock samples showed stress-strain behavior which was more similar to that of soils than competent rocks, exhibiting large permanent deformations with frictional slip. The mechanical behavior of the samples approached that of competent rocks as the amount of binder was increased. For very weak samples, acoustic waves propagating in these rocks showed very low velocities of less than 1000 m/sec for compressional waves. A borehole made within this weakly cemented rock exhibited a unique mode of failure that is called "anti-KI mode fracture" in this paper. The effect of cementation, grain type, and boundary conditions on this mode of failure was also examined experimentally.

1 INTRODUCTION

Rocks with weak intergranular cementation are often encountered during drilling and excavation in poorly consolidated, young, geological formations. Because the strength of such materials is low, they can be a potential threat to the stability of boreholes and other stress-bearing rock structures. They are, however, difficult to characterize because their mechanical behavior is intermediate between that of rock and soil.

One of the fundamental differences between granular rock (sandstone) and soil (sand) is the strength of intergranular cohesion. Due to the lack of cohesion, sand under differential stress exhibits significant permanent deformation due to intergranular slip and rotation that overwhelms the elastic deformation of the grains and grain contacts. A number of theories have been developed to predict the nonlinear, hysteretic stress-strain behavior of sands from only the grain packing geometry and frictional properties between grains (e.g., Mehrabadi et al., 1992; Nemat-Nasser & Balendran, 1992). In contrast, deformation of competent sandstone (such as Berea) consists of both elastic deformation of grains and grain contacts and frictional slip between grains. The contribution from frictional slip can be significant (e.g. Nihei et al., 2000) but it is mostly recoverable during unloading. Intergranular cohesion allows the transmission of macroscopic tensile stress in the medium that can lead to the formation of tensile fractures. Weakly cemented granular rocks are expected to show intermediate behavior between sand and competent sandstone, exhibiting strongly hysteretic stress-strain behavior and the ability to sustain intergranular extensile fractures.

The objective of this study is to understand the effect of the micromechanical properties of weak granular rock such as intergranular cohesive strength and porosity on macroscopic properties including load-displacement response, ultimate strength, acoustic wave velocities, and failure mode. To this end, we conducted laboratory experiments upon synthetic samples of weakly cemented sandstone with a range of micromechanical properties. The synthetic rock samples were fabricated of pure silica sand with smooth, elongated grain geometry. The grains were cemented by sodium silicate. A series of laboratory load-displacement tests and acoustic wave propagation tests were performed both on core samples and rectangular bricks containing a single simulated borehole. The primary micromechanical parameter used for a series of experiments was the strength of intergranular cohesion. Porosity of the samples was also varied but its range was limited to relatively high values (32-42%). For the brick samples containing a simulated borehole, samples were also made of glass beads (nearly perfectly spherical) to examine the effect of grain geometry.

2 ARTIFICIAL SANDSTONE SAMPLES

Artificial rock samples were fabricated by cementing grains of pure silica sand and glass beads with a small amount of sodium silicate solution. For cemented silica-sand samples used for stress-strain and acoustic tests, the grain size was 0-250 μm, 76% between 150-215 μm, fines (<75μm) 0.6%. For both silica-sand and glass-bead brick samples with a simulated borehole, the grain size was 150-215 μm. Both silica sand and glass bead grains were first evenly coated with a carefully measured amount of sodium silicate aqueous solution. The cement-grain mixture was then compacted in a mold to achieve a desired porosity (ϕ). Next, the compacted samples were dried to establish intergranular bonds. Once dried, the volume of sodium-silicate solution reduced to approximately 50% of the original. Throughout this paper, the amount of cement used in each sample is indicated by saturation ratio S=[dry sodium silicate cement volume]/[pore volume]x100 (%).

The cohesive strength between grains and porosity were controlled by changing the amount of sodium silicate and the degree of compaction, respectively. Because the amount of sodium silicate required to bond grains was very small, the porosity and the cohesion strength are considered as independent parameters for most of the samples.

3 UNIAXIAL COMPRESSION TESTS

3.1 *Experimental setup*

Uniaxial compression tests were conducted upon cylindrical samples of cemented silica sand. Samples were 2 inches (5.08 cm) in diameter and 6 inches (15.24 cm) tall. Experimental setup is shown in Figure 1. Because samples with small cement volume were very friable and the failure tended to initiate at the sample-loading plate interface, end sections of each sample were made of higher-strength material that contained a relatively larger volume of cement (pore saturation ratio S=2.5 %).

3.2 *Effect of intergranular cohesive strength*

A series of uniaxial compression tests was conducted upon samples with a constant porosity (ϕ =38%). The results showed that until the grains achieved a certain level of intergranular cohesion, samples with different cementation followed an identical load-displacement path, but with different ultimate strengths (Uc's) and deformation. Once this critical cohesion was achieved, deformation due to intergranular slip decreased monotonically and the behavior became rock-like (Figure 2).

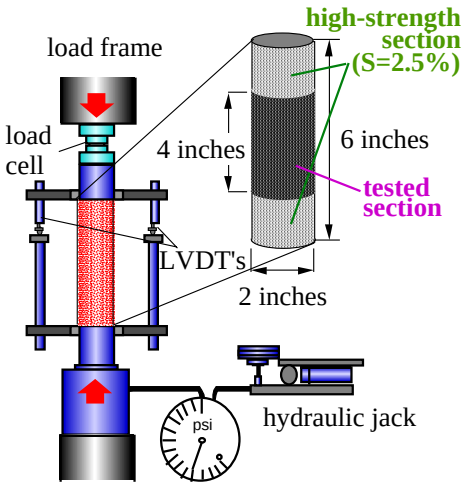

Figure 1. Experimental setup for uniaxial compression test. Samples have sections of higher-strength material to prevent failure initiation at loading plate interfaces.

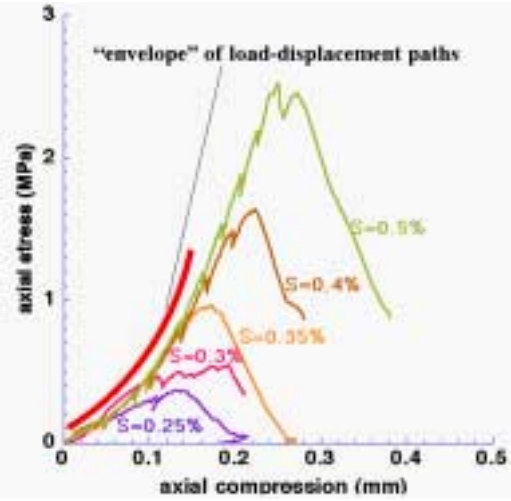

(a) S<0.5%

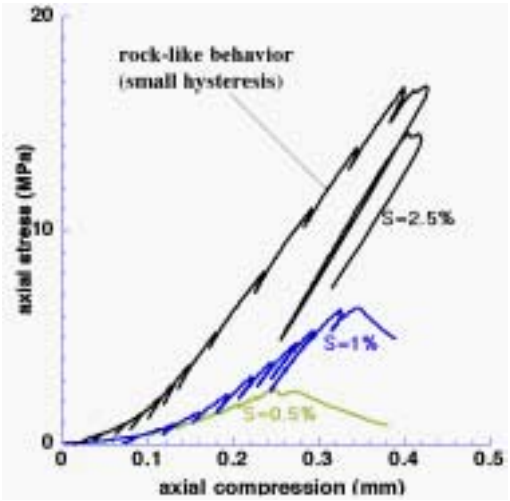

(b) S>0.5%

Figure 2. Load-displacement behavior of samples with a range of intergranular cementation. The displacements in the

horizontal axis include deformation within the higher-strength sections (S=2.5%).

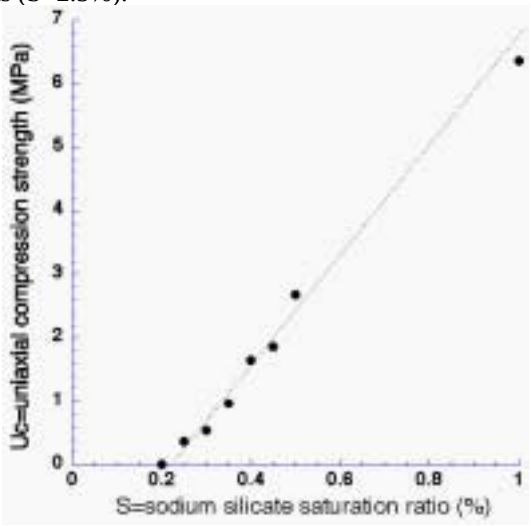

Figure 3. Ultimate strength of uniaxially loaded artificial sandstone samples. After a threshold concentration of S=0.2% is reached, Uc increases linearly with S.

Interestingly, samples did not show any cohesion until S~0.2%. Although the reason for this behavior is not apparent, it may be related to the formation of a film on sand grains that required a minimum amount of sodium silicate solution. Once this threshold was cleared, uniaxial compression strength increased linearly with cement volume up to Uc=2 MPa (Figure 3).

3.3 *Effect of porosity*

For a constant cement volume (S=0.5%), samples with three different porosities (ϕ =32, 35, and 39%) were tested. The load-displacement behavior of these samples were similar but Uc decreased with increasing porosity (Figure 4).

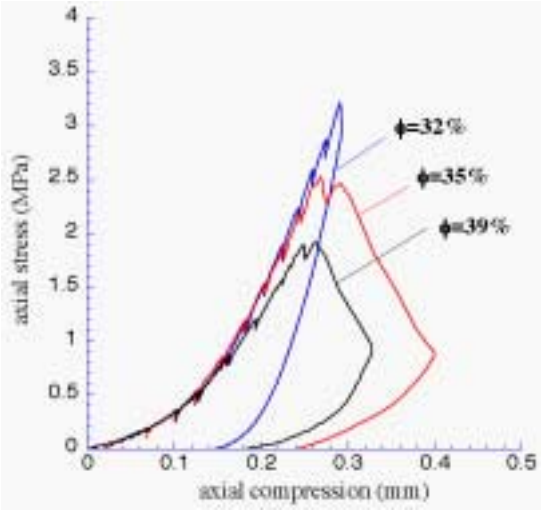

Figure 4. Load-displacement behavior of weakly cemented silica sand samples for different porosities. Sodium silicate aqueous solution content was S=0.5% for all three samples.

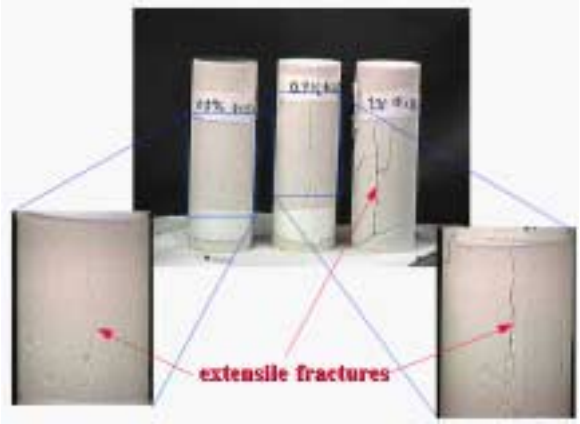

Figure 5. Exensile fractures formed during uniaxial compression tests. From left to right, cement content of the samples was S=0.25, 0.35, and 0.5 % (Uc=0.37, 0.97, and 2.7 Mpa). The numbers on the samples are given in sodium silicate aqueous solution volume (C=2xS).

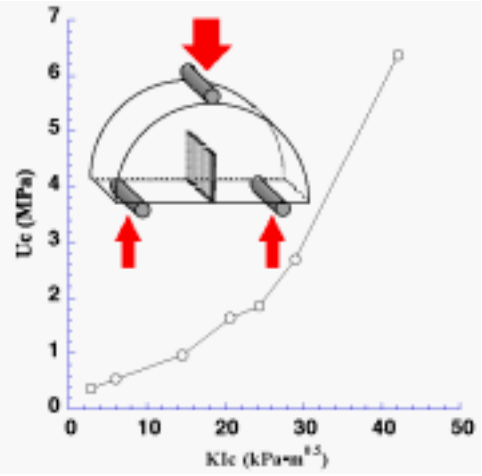

Figure 6. KIc fracture toughnesses determined using a modified half-disc three point bending test.

3.4 . *KI fracture toughness*

Despite a large change in Uc over the range in cement content, all samples failed exhibiting clear extensile mode fractures (Figure 5). This indicates that only a small amount of intergranular cohesion is required to create tensile fractures within a granular medium. The KI toughness (tensile fracture toughness) of the samples for ϕ =35% samples was determined by a modified three point bending test with a notched 2" diameter half-disc sample (e.g., Whittaker et al., 1992). Notch width was less than 1 mm and the span length between bottom supports was 0.8x D (specimen diameter). Values of KIc (not corrected for sample geometry) were computed by the equation derived by Chong et al. (1987) and plotted against Uc's in Figure 6 using the relationship given in Figure 3.

As the plot indicates, values of KIc for the artificial weak rocks are very low compared to well cemented granular rock; Whittaker et al., (1992) reports a value of 380 kPa•m $^{0.5}$ for sandstone obtained by the same method. All the weak rock samples failed in the same manner as expected for a strong rock: unstable propagation of a fracture starting at the top of the notch. No microscopic observations were made of the zone at the tip of the fracture. There appears to be a nearly linear relationship between KIc and Uc for S's below 0.5%.

4 ACOUSTIC TESTS

4.1 *Experimental setup*

Acoustic measurements were conducted using short cylindrical samples of 2 inches (5.08 cm) in diameter and 2 inches in length. Both dry and liquid saturated samples were used. Isopropyl alcohol of 99% purity was used as pore fluid because sodium silicate cement dissolves in water.

For dry samples, both P and S-waves transmitted through the samples were measured. Central frequency of the seismic transducers (Panametrics, Inc.) was 500 kHz for P-wave and 250 kHz for S-wave. For liquid-saturated samples, only P-waves were measured using transducers with three different central frequencies (f_c=100 kHz, 500 kHz, and 1 MHz).

4.2 *Results for dry samples*

For dry samples, approximately 0.08 MPa of stress was applied through a thin piece of lead foil to achieve good consistent acoustic coupling between the seismic transducers and a sample. Both P and S-wave velocities and amplitudes increased significantly with increasing intergranular cementation (Figure 7 a and b). Despite the large changes in velocities over a range of cementation, dynamic Poisson's ratio determined from P and S-wave velocity ratio remained virtually constant, at about 0.13 (Figure 8). This result is interesting because it indicates a possibility of a unique relationship between porosity and Poisson's ratio of a cemented granular medium.

P and S-wave velocities were also measured for a solid, thin disk sample of desiccated sodium silicate cement. These data were used, along with known properties of the silica sand and estimates of the cement volume fraction, as input to the micromechanical model of Dvorkin and Nur (1996) for the effective bulk moduli (K) of cemented sandpacks. The measured results showed good agreement with predictions by a model that assumes a coating of cement around individual grains (Figure 9). This model is called "Scheme 2" while the "Scheme 1" model assumes cementing material only at grain contact). This result is consistent with the way in which the samples were made: the cement and sand were uniformly mixed before compaction and cementation of the sample.

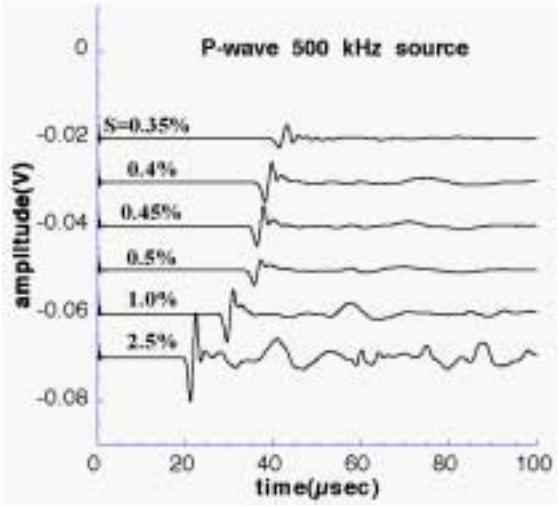

(a) P-waves

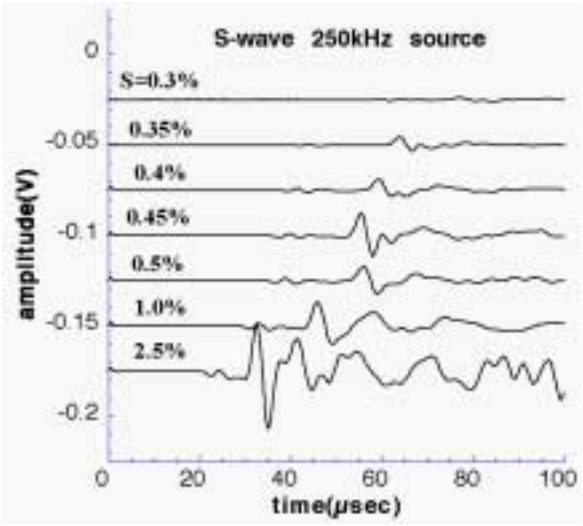

(b) S-waves

Figure 7. Measured seismic waveforms for cemented silica sand samples under room-dry condition. Transducer's central frequency was 500 kHz for P-waves and 250 kHz for S-waves.

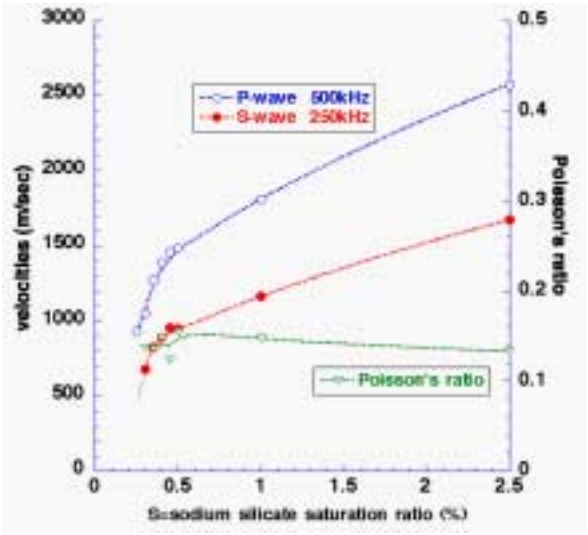

Figure 8. P and S-wave velocities determined from waveforms in Figure 7. Dynamic Poisson's ratio for these velocities are also shown as a function of pore saturation ratio by cement, S.

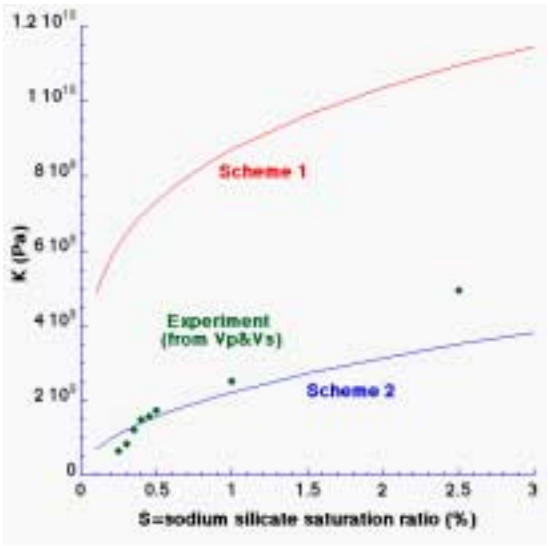

Figure 9. Comparison of experimental bulk moduli determined from ultrasonic velocity measurements and theoretical predictions by Dvorkin-Nur models.

4.3 *Results for liquid-saturated samples*

Samples vacuum-saturated with 99% pure isopropyl alcohol were tested with P-wave pulses with three different central frequencies of 100 kHz, 500 kHz, and 1 MHz (Figure 10). An increase in P-wave ("fast" P-wave) velocity with increasing cement volume similar to the dry samples was observed. The general behavior of velocity for liquid-saturated samples could be predicted from dry P and S-wave velocities using the classical Biot's model (results for 500 kHz waves are shown in Figure 11). However, samples with weak intergranular cohesion showed very strong attenuation of high-frequency waves (Figure 10c) that could not be predicted by the theory. Also, the velocity dispersion of P-waves between 100 kHz and 1 MHz was much larger than the theoretical prediction. The observed attenuation and dispersion of P-wave may be explained by the possible formation of sand grain clusters that were more poorly cemented than surrounding grains. For such velocity anomalies, high-frequency waves are attenuated by scattering and propagate along the fastest path that detours around the clusters.

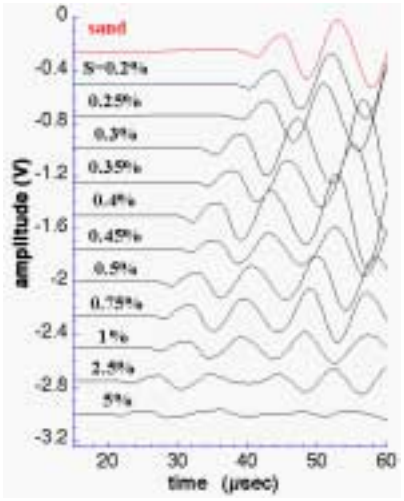

(a) 100 kHz P-wave

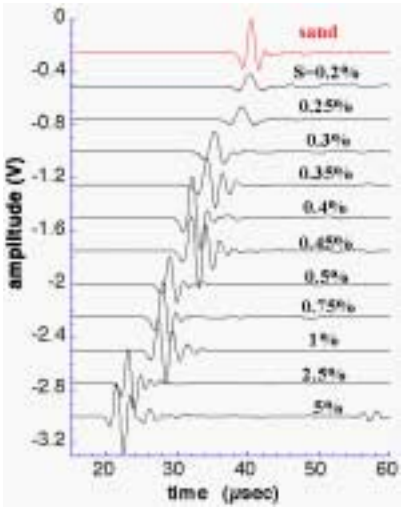

(b) 500 kHz P-wave

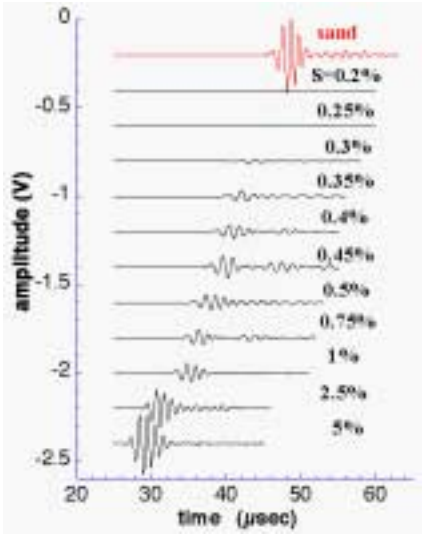

(c) 1 MHz P-wave

Figure 10. P-wave waveforms measured for isopropyl alcohol saturated cemented silica sand samples.

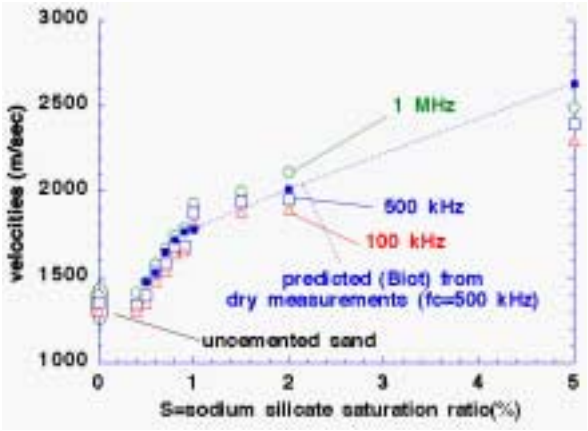

Figure 11. Velocities of P-waves determined for waves shown in Figure 10. Predictions by Biot's theory are shown for waves generated by a 500 kHz source.

5 BOREHOLE BREAKOUT TESTS

5.1 *"Non-dilatational" fracture*

In recent years, boreholes in weakly cemented granular rocks with high porosity have been shown to exhibit a unique mode of failure (e.g. Bessinger et al., 1997). Similar to the classical borehole breakout, this failure occurs in a host rock surrounding a borehole in the direction of minimum principal stress. However, unlike the classical breakout that occurs as a collection of extensile fractures aligned parallel to the borehole wall in the maximum compressive principal stress direction (Ewy and Cook, 1990a, b), this failure in weak granular rocks develops as a single slit in the direction perpendicular to the wall (Figure 12). This type of failure can be a great threat to the stability of a borehole because the inflow of broken rock fragments from a propagating slit tip does not stop in contrast to the classical breakout that tends to stabilize.

Based on their laboratory experiments on sintered glass-bead bricks and numerical experiments of Liu (1995), Bessinger et al. called this failure a "non-dilatational" fracture because compaction and/or removal of debonded and crushed grains was essential for the formation of such failure. In this paper, we call it an "anti-KI mode" fracture in contrast to the usual KI mode fracture that develops in the maximum compressive principal stress direction.

5.2 *Experimental setup*

Rectangular bricks of cemented sand and glass beads containing a single through-going hole were uniaxially compressed to observe borehole breakout (Figure 13). The bricks were 8 inches tall, 4 inches wide, and 1.1 inch deep. The diameter of the hole was 0.9 inches. Before loading, a pair of chevron notches were made at the top and bottom of the hole to prevent shock loading from unstable propagation of vertical KI (splitting) fractures during the test. Also, plastic face plates were taped to the front and back surfaces of the samples in order to prevent the ejection of debonded and crushed grains.

5.3 *Results for glass-bead bricks*

For glass bead bricks, the anti-KI mode fracture was formed for all tested samples (S=0.5-2.5%). With increasing axial load, vertical extensile fractures were first formed along the chevron notch. Next, the sides of the hole started to crumble and then a pair of horizontal notches (anti-KI fractures) propagated perpendicular to the borehole wall (Figure 14a). The range of Uc for these samples was 2.5-11.5 MPa and the porosity was approximately 42%. Although Uc of the samples varied significantly, cement content had no apparent effect on the failure pattern described above.

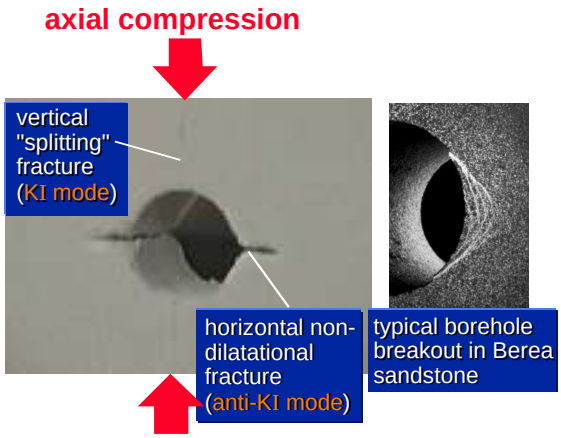

Figure 12. Anti-KI mode (or "non-dilatational") fracture in weakly cemented granular medium.

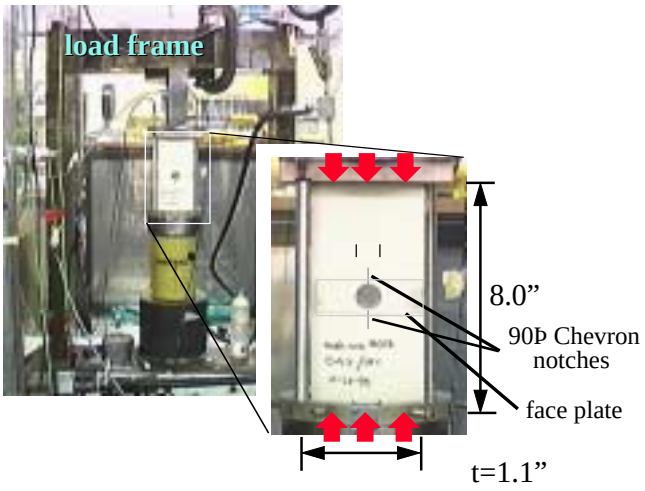

Figure 13. Experimental setup for uniaxial compression tests on brick samples with a single simulated borehole.

Subsequently, identical samples were tested with a thin plastic liner applied to the interior of the borehole. This liner prevented the ejection of failed grains into borehole. For these samples, conical zones of debonded and compacted grains were formed in the horizontal direction instead of a thin notch-like failure of anti-KI fractures (Figure 14b). Further loading resulted in spalling of surfaces, followed by the catastrophic failure of sample due to the propagation of vertical fractures from the edge of the conical zones. The width of conical failure at the borehole wall was 10-20 grain size in contrast to 5-10 grain size of anti-KI fracture.

5.4 *Results for silica sand bricks*

Uniaxial compression tests were also conducted on bricks of cemented silica sand containing a borehole. Only samples with cement content S=2.5% and 10% were tested. Porosity of the samples ignoring the reduction due to the desiccated cement was 39%. It should be noted that for S=10% sample, the reduction in porosity due to sodium silicate cement was not negligible (apprximately 4%).

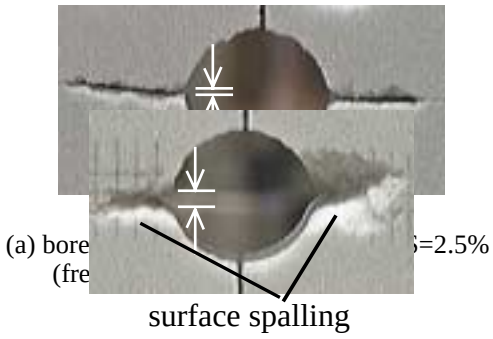

(b) borehole breakout with lining, S=2.5% (grain ejection prevented)

Figure 14. Effect of borehole lining preventing the formation of anti-KI fractures. In the bottom photograph, the plastic liner and debonded grains were removed after the test.

For S=2.5% sample, in contrast to glass bead bricks, the anti-KI fracture was not formed (Figure 15a). The failure which occurred in this sample was similar to the conical failure zone in the bead brick with a plastic liner in a borehole. It was also confirmed that only a small amount of debonded sand grains was ejected into the borehole even though no attempt was made to prevent their movement. It appeared that this was due to the interlocking of nonspherical sand grains and also the smaller porosity of the sand pack than the bead pack.

Next, an identical sample (S=2.5%, Uc~13 MPa) was uniaxially loaded. This time, however, we used flow of compressed air to dislodge debonded grains from the borehole wall. As the debonded grains were removed, narrow horizontal notches that are characteristic of anti-KI fractures propagated (Figure 10b). This continued until the grains which were trapped between fracture walls came into contact under load and the sample failed catastrophically due to the growth of vertical fractures from the notch tips.

Finally, a sample with a much larger cement content (S=10%) was tested. Uniaxial compression strength for this sample was not measured but was expected to be much higher than the S=2.5% sample. Again, an attempt was made to dislodge debonded grains using compressed air but only a small amount of grains could be removed. In addition to the conical failure zone similar to the case without grain removal, failure of the borehole wall for this sample showed propagation of extensile fractures along borehole wall as well as crushing of individual sand grains. This mode of failure is known as classical borehole breakout.

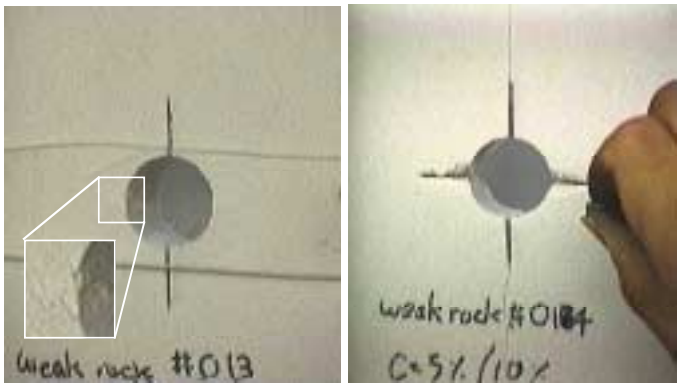

(a) S=2.5%. (b) S=2.5%. Grains removed by compressed air

(c) S=10%. Extensile fractures in borehole wall were observed.

Figure 15. Borehole failure in cemented silica sand bricks

6 CONCLUSIONS

Results of mechanical tests showed linear relationships among intergranular cementation, uniaxial compression strength, and KI fracture toughness for samples with small cement content. For these samples, stress-strain behavior is

characterized by large permanent deformation that is caused by intergranular slip and grain rotations.

Acoustic measurements revealed a significant, nonlinear increase in both P and S-wave velocities for dry samples with increasing intergranular cementation. Despite this large change, dynamic Poisson's ratio did not change for a given porosity of the rock. Bulk elastic moduli computed from these velocities showed good agreement with the theoretical predictions by one of the Dvorkin-Nur cemented grain models.

The experimental results for the failure of a simulated borehole within cemented glass bead and silica sand demonstrate the importance of grain mobility for the formation of anti-KI fractures. The mobility is high if a rock has a high porosity, rounded grains, small intergranular friction and cohesion. In addition to these factors, external driving forces such as mechanical vibration and fluid flow assist the removal of grains from the fracture tip. Similar properties and processes would be relevant to boreholes and tunnels excavated within weakly cemented granular rock. Because of the large impact of anti-KI mode failure upon the stability of structures in rock, further research is required to determine quantitative relationships between relevant micromechanical parameters of rock and the mode of failure under given boundary conditions.

Throughout this study, use of artificial rock enabled a careful examination of the effect of intergranular strength on uniaxial strength, fracture toughness, ultrasonic properties, and failure mode of a borehole in weak granular rock. The relevance of the observed behavior to naturally occurring weak rocks depends partly on whether the type of cement providing the intergranular strength affects behavior. Further tests need to be conducted to evaluate this.

ACKNOWLEDGMENT

Authors would like to thank Dr. Robert W. Zimmerman at T.H.Huxley School, Imperial College, London, UK for theoretical calculations of Dvorkin-Nur models and insightful discussions. Support for this work was provided by the Director, Office of Science, Office of Basic Energy Sciences, Geosciences, Geoscience program, under the U.S. Department of Energy Contract No. DE-AC03-76SF00098.

REFERENCES

Bessinger, B.A., Liu, Z., Cook, N.G.W., & Myer, L.R. 1997. A new fracturing mechanism for granular media. *Geophys. Res. Lett.* 24(21): 2605-2608.

Chong, K.P., Kuruppu, M.D. & Kuszmaul, J.S. 1987. Fracture toughness determination of rocks with core-based specimens. In Shah S.P. & Swartz S.E.(eds.*), SEM/RILEM Int. Conf. on Fracture of Concrete and Rock*. Houston. Texas: 9-15.

Dvorkin, J. & Nur, A. 1996. Elasticity of high-porosity sandstones: Theory for two North Sea datasets. *Geophys*. 61: 1363-1370.

Ewy, R.T. & Cook, N.G.W. 1990a. Deformation and fracture around cylindrical openings in rock -I. Observations and analysis of deformations. *Int. J. Rock Mech. Min. Sci. & Geomech. Abstr*. 27: 387-408.

Ewy, R.T. & Cook, N.G.W. 1990b. Deformation and fracture around cylindrical openings in rock -I. Initiation, growth and interaction of fractures. *Int. J. Rock Mech. Min. Sci. & Geomech. Abstr*. 27: 409-427.

Liu, Z. 1995. Numerical simulation of microscopic deformation and failure of clastic media. Ph.D.dissertation. University of California at Berkeley.

Mehrabadi, M.M., Loret, B. & Nemat-Nasser, S. 1992. A constitutive model for granular materials based on micromechanics, In Shen H.H. et al.(ed.), *Advances in Micromechanics of Granular Materials*. 81-90. Amsterdam: Elsevier.

Nemat-Nasser, S. & Balendran, B. 1992. Micromechanics of flow and failure modes of particulate media over a wide range of strain rates, In Shen H.H. et al.(eds.), *Advances in Micromechanics of Granular Materials*. 21-30. Amsterdam: Elsevier.

Nihei, K.T., Hilbert, Jr., L.B., Cook, N.G.W., Nakagawa, S. & Myer, L.R. 2000. Frictional effects on the volumetric strain of sandstone. *Int. J. of Rock Mech. & Min. Sci*.. 37(1-2): 121-132.

Whittaker, B.N., Singh, R.N., & Sun, G. 1992. *Rock Fracture Mechanics, Developments in Geotechnical Engineering* 71, New York: Elsevier